Computers in Biology and Medicine 113 (2019) 103409

Contents lists available at ScienceDirect

Computers in Biology and Medicine

journal homepage: www.elsevier.com/locate/compbiomed

# A three-dimensional quantification of calcified and non-calcified plaques in coronary arteries based on computed tomography coronary angiography images: Comparison with expert's annotations and virtual histology intravascular ultrasound

Vassiliki I. Kigka[a,b], Antonis Sakellarios[a,b], Savvas Kyriakidis[a,b], George Rigas[a,b], Lambros Athanasiou[c], Panagiotis Siogkas[a,b], Panagiota Tsompou[a], Dimitra Loggitsi[d], Dominik C. Benz[e], Ronny Buechel[e], Pedro A. Lemos[f,g], Gualtiero Pelosi[h], Lampros K. Michalis[i], Dimitrios I. Fotiadis[a,b,*]

[a] Unit of Medical Technology and Intelligent Information Systems, Department of Materials Science and Engineering, University of Ioannina, GR 45110, Ioannina, Greece
[b] Institute of Molecular Biology and Biotechnology, Dept. of Biomedical Research Institute – FORTH, University Campus of Ioannina, GR 45110, Ioannina, Greece
[c] Institute for Medical Engineering and Science, Massachusetts Institute of Technology, Cambridge, MA, 02139, United States
[d] CT/MRI Department, Hygeia & Mitera Hospitals, Athens, Greece
[e] Department of Nuclear Medicine, Cardiac Imaging, University Hospital Zurich, Ramistrasse 100, 8091, Zurich, Switzerland
[f] Dept. of Interventional Cardiology, Heart Institute, University of São Paulo Medical School, São Paulo-SP, 05403-000, Brazil
[g] Dept. of Interventional Cardiology, Hospital Israelita Albert Einstein, Sao Paulo-SP, 05652-000, Brazil
[h] Institute of Clinical Physiology, National Research Council, Pisa, IT 56124, Italy
[i] Dept. of Interventional Cardiology, Medical School, University of Ioannina, GR 45110, Ioannina, Greece

ARTICLE INFO

*Keywords:*
Computed tomography coronary angiography
Coronary artery disease
Atherosclerotic plaque
Calcified plaque
Non-calcified plaque
Segmentation
Active contour models

ABSTRACT

The detection, quantification and characterization of coronary atherosclerotic plaques has a major effect on the diagnosis and treatment of coronary artery disease (CAD). Different studies have reported and evaluated the noninvasive ability of Computed Tomography Coronary Angiography (CTCA) to identify coronary plaque features. The identification of calcified plaques (CP) and non-calcified plaques (NCP) using CTCA has been extensively studied in cardiovascular research. However, NCP detection remains a challenging problem in CTCA imaging, due to the similar intensity values of NCP compared to the perivascular tissue, which surrounds the vasculature. In this work, we present a novel methodology for the identification of the plaque burden of the coronary artery and the volumetric quantification of CP and NCP utilizing CTCA images and we compare the findings with virtual histology intravascular ultrasound (VH-IVUS) and manual expert's annotations. Bland–Altman analyses were employed to assess the agreement between the presented methodology and VH-IVUS. The assessment of the plaque volume, the lesion length and the plaque area in 18 coronary lesions indicated excellent correlation with VH-IVUS. More specifically, for the CP lesions the correlation of plaque volume, lesion length and plaque area was 0.93, 0.84 and 0.85, respectively, whereas the correlation of plaque volume, lesion length and plaque area for the NCP lesions was 0.92, 0.95 and 0.81, respectively. In addition to this, the segmentation of the lumen, CP and NCP in 1350 CTCA slices indicated that the mean value of DICE coefficient is 0.72, 0.7 and 0.62, whereas the mean HD value is 1.95, 1.74 and 1.95, for the lumen, CP and NCP, respectively.

## 1. Introduction

Atherosclerosis, the underlying cause of coronary artery disease (CAD), accounts for a significant portion of deaths and is considered as a principal cause of mortality and morbidity worldwide [1]. The established modalities used to identify and specify the atherosclerotic plaque characteristics include the Intravascular ultrasound (IVUS) and the Optical Coherence Tomography (OCT), which appear in many

* Corresponding author. Unit of Medical Technology and Intelligent Information Systems, Dept. of Materials Science and Engineering, University of Ioannina, PO Box 1186, GR 451 10, Ioannina, Greece.
*E-mail address:* fotiadis@cc.uoi.gr (D.I. Fotiadis).

https://doi.org/10.1016/j.compbiomed.2019.103409
Received 25 April 2019; Received in revised form 23 August 2019; Accepted 23 August 2019
Available online 27 August 2019
0010-4825/ 

studies as the ideal approaches to study the atherosclerosis evolution. However, due to their invasive nature, they are time consuming and involve a considerable patient risk. In contrast, the recent technology advancements in non-invasive imaging and spatial resolution improvement allow the accurate diagnosis of CAD [2]. Computed Tomography Coronary Angiography (CTCA) is a promising non-invasive imaging modality, which is able to detect the inner and the outer wall of coronary arteries, the luminal stenosis and also permits the characterization of the atherosclerotic plaque composition into CP and NCP. In addition to this, CTCA allows the assessment of atherosclerotic disease in the entire coronary arterial tree and the identification of high risk plaques, including spotty calcifications, low HU attenuation plaques and napkin-ring sign [3]. Therefore, the ability of CTCA to identify atherosclerotic plaque features with increased vulnerability provides information for both high-risk and low-risk patients [4].

As far as the atherosclerotic plaque detection methodologies is concerned, different approaches have been proposed for the identification either of CP and NCP or of mixed atherosclerotic plaques, which are mainly based on Hounsfield Units (HU) analysis. More specifically, Voros et al. [5] characterized plaque burden region pixels as CP, high density NCP and low density NCP, after the implementation of an HU based analysis and evaluated their findings using IVUS modality. In the same rationale, Dey et al. [6] implemented a threshold scan-specific based method to quantify 22 NCP plaque volumes using an automated computer software (AUTOPLAQ) and evaluated its performance with manual plaque quantification performed by experts, using the IVUS imaging modality. An HU based analysis was also applied in another study, proposed by Brodoefel et al. [7], who attempted to accurately identify the NCP pixels.

This study was validated in 22 lesions, in 14 patients, comparing the proposed HU-based analysis with Virtual Histology Intravascular Ultrasound (VH-IVUS). The studies in Refs. [8,9] indicated also a good correlation between coronary CTCA and IVUS for plaque measurements. Graaf et al. [10] studied the correlation between the plaque volume derived by CTCA automatic software (QAngio CT 1.1, Medis medical imaging systems) and the plaque volume provided by VH-IVUS, which was considered as the gold standard. In their study, the fixed intensities threshold and the adaptive threshold technique, according to luminal contrast densities, were implemented to classify the atherosclerotic plaque into fibrotic tissue, fibrofatty tissue, necrotic core and calcium. A different approach was proposed by Jawaid et al. [11], who implemented a support vector machine (SVM) classifier, after computing the radial profiles by averaging the CTCA image intensity in rings around the vessel centerline to identify the abnormal coronary segments. A derivative-based method was also applied to localize the position and the length of the NCP.

In this study, we present the technical development of CTCA modality to identify the lumen, the outer wall, the CP and NCP accurately as such invasive IVUS modality performs. We examine the accuracy of the CTCA modality to detect the coronary inner wall boundaries and to identify the plaque burden region and specify the atherosclerotic plaque composition. More specifically, an active contour model which incorporates a prior shape methodology was utilized for the lumen segmentation, whereas the identification and volumetric quantification of CP and NCP was achieved, using density measurements, quantified by Hounsfield units. The detection of CP is achieved by an active contour based model, whereas the NCP is detected by an adaptive threshold based technique. Both the detection of CP and the NCP threshold values definition and the direct comparison of CP and NCP segmentation with manual expert's annotations as well constitute the novelty of the present study.

Based on the concept that the absolute HU range of both CP and NCP plaques is significantly affected by the dose protocol selection and the luminal density [12], our approach is fully adaptive to each acquisition dose protocol methodology for the detection of CP and NCP, as well as their 3D models construction. The proposed methodology is evaluated using both manual annotations in 2D CTCA slices and using the VH-IVUS imaging modality, which is considered a well established invasive modality for the detection and characterization of atherosclerotic plaques and has been extensively utilized in different existing studies as the gold standard of atherosclerotic plaques detection [13,14]. Moreover, based on existing studies in which VH-IVUS has been directly compared to histology [15,16], VH-IVUS modality is considered as a safe imaging modality to be used as gold standard in our proposed methodology. This approach was implemented in the entire arterial tree and was applied in an automated manner, requiring the minimal user interaction to annotate the starting point of coronary artery bifurcation and the ending points of the coronary artery branches.

## 2. Methods

### 2.1. Proposed methodology

The proposed methodology includes seven steps. In the first step, a pre-processing procedure is implemented to detect the potential vessel region. In the second step, a blooming effect removal technique is implemented to improve the CTCA image quality in the high intensity regions. In the third step, the artery centerline is extracted. In the fourth step, three different weight functions for the lumen, the outer wall and the CP are estimated to approximate the potential HU values ranges for the lumen, the outer wall and CP. In the fifth step, an extended approach of active contour models without edges is implemented to detect the inner wall, the outer wall and the CP. In the sixth step, an adaptive intensity range is extracted based on the mean lumen intensity for the detection of NCP. Finally, in the seventh step, the 3D geometrical models for the inner and, the outer wall, the CP and the NCP are constructed, employing the fast marching cubes approach.

#### 2.1.1. Preprocessing

The CTCA image preprocessing step includes the implementation of a vessel enhancement preprocessing technique [17], which searches for geometrical structures, regarded as tubular. The implemented filter aims to construct a multiscale representation of vascular imaging data that could effectively be implemented for multiscale approaches to vascular image analysis, through preserving the vessel diffusion. The diffusion process is regulated through the analysis of the eigensystem of the Hessian matrix and based on the calculated eigenvalues, the CTCA image vesselsness measure is estimated. More specifically, in this methodology an improved smoothed version of the typical vesselness measure, proposed by Frangi et al. [18], is utilized and its formulation is:

$$V = \begin{cases} 0, & if\ \lambda_1 > 0\ or\ \lambda_2 > 0 \\ \left(1 - e^{-\frac{A^2}{2\alpha^2}}\right) e^{-\frac{B^2}{2\beta^2}} \left(1 - e^{-\frac{S^2}{2\gamma^2}}\right), & otherwise \end{cases} \tag{1}$$

where $A = \frac{|\lambda_2|}{|\lambda_3|}$ differentiates between pate and line like structures, $B = \frac{|\lambda_1|}{\sqrt{|\lambda_2 \lambda_3|}}$ respects to the deviation from a blob like structure, $S = \sqrt{\lambda_1^2 + \lambda_2^2 + \lambda_3^2}$ differentiates the foreground (vessel) from the background and the parameters $\alpha$, $\beta$, $\gamma$ are considered as weighting factors, which control the influence of $A$, B and $S$. In Fig. 1 we show an example of the utilized filter implementation.

#### 2.1.2. Blooming effect removal

The blooming effect is a typical CTCA image artifact, where small high density objects are thicker with smeared edges. This artifact affects the visualization and the quantification of small structures, such as the calcifications, as well as, the visualization of metal stents. Thus, in this

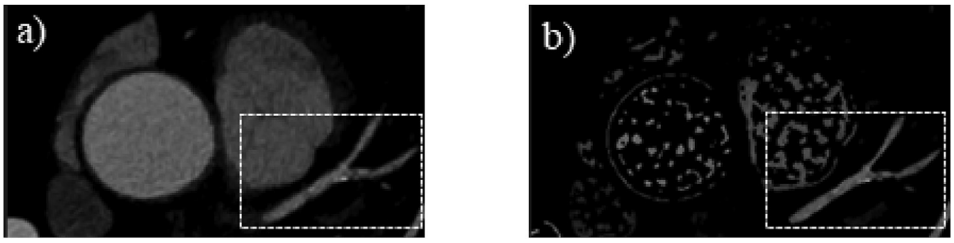


**Fig. 1.** Frangi Vesselness filter (a) before implementation (b) after implementation.

step we aim to remove the blooming effect, by applying the Blind deconvolution approach [19]. In general, an output CTCA image can be modeled by the convolution of the deblurred input image with the point spread function (PSF) of the system as:

$$f(x, y) = g(x, y) * h(x, y) \tag{2}$$

where $h(x, y)$ corresponds to the PSF of the CT system, $g(x, y)$ is the real input structure and $f(x, y)$ represents the output image. The PSF of the CTCA scanners varies between different scanners and thus different approaches have been utilized for the PSF estimation. In our methodology, we assume that the PSF is estimated as a simple Gaussian kernel as proposed in different existing in the literature studies [20,21] and subsequently we implement on the high intensities CTCA image's regions a deconvolution technique to acquire the deblurred CTCA image [22]. In Fig. 2, we show a typical implementation of deconvolution approach.

### 2.1.3. Centerline extraction

In this step, a minimum cost path approach, based on the Metz et al. [23] study is implemented to extract the coronary vessel centerline. The coronary vessel centerline is required to create an initial coronary vessel mask. This is a simple approach, since its implementation requires only the starting and the ending point of the coronary vessel and an estimation of a minimum cost function. The considered cost function $(C(\vec{x}))$ is a combination of the vesselness measure and an intensity based measure and it is described as:

$$C(\vec{x}) = \frac{1}{V(\vec{x})T(\vec{x}) - \varepsilon} \tag{3}$$

where $V(\vec{x})$ is the vesselness measure proposed by Manniesing et al. [17], $T(\vec{x})$ is a lumen intensity measure and $\varepsilon$ is a small positive factor which avoids errors of singularity of $C(\vec{x})$, when $V(\vec{x})T(\vec{x}) \rightarrow 0$. The lumen intensity membership function is described as a combination of two sigmoidal functions, which are defined as:

$$f_{sigm}(x; a, c) = \frac{1}{1 + e^{-a(x-c)}} \tag{4}$$

where $x$ is the input intensity image and $a, c$ are parameters, which control the steepness and center of the transformation function, respectively. The final lumen membership function is:

$$f_{lumen}(x; a, c) = f_{sigm}(x; a_{1,lumen}, c_{1,lumen}) \times f_{sigm}(x; a_{2,lumen}, c_{2,lumen}) \tag{5}$$

Where $a_{1,lumen} = 0.02$, $c_{1,lumen}$ is the minimum value between $ml - l_{thres}$ and 500, $a_{2,lumen} = -0.01$ and $c_{2,lumen}$ corresponds to the $ml + cp_{thres}$. The threshold of the lumen ($l_{thres}$) and the calcified plaques ($cp_{thres}$) was defined heuristically 80 HU and 400 HU, respectively, whereas the mean luminal intensity ($ml$) corresponds to the value of the highest 50% of the image intensities values, which are higher than 100 HU and considering only the vessel candidate parts of the image ($V(\vec{x}) > 0$). Subsequently, the shortest distance from a list of points to all other pixels in an image volume is calculated based on a Multistencil Fast Marching method (MSFM).

### 2.1.4. Estimation of weight function for lumen, outer wall and calcified plaque

In this step, three different membership functions for the lumen ($f_{lumen,updated}$), the outer wall ($f_{outer}$) and the CP ($f_{CP}$) were estimated, aiming to compensate different protocols for discriminating the lumen, the outer wall and the CP. Contrary to the CP intensity ranges, the NCP intensity ranges are close to the outer wall HU values and as a result, a membership function cannot be extracted for the NCP detection. The utilized membership functions are all adapted to each CTCA image and are formulated as:

$$f_{lumen,upated} = (1 - \varepsilon)(f_{sigm}(x; a_{1,lumen}, c_{1,lumen}) \times f_{sigm}(x; a_{2,lumen}, c_{2,lumen})) + \varepsilon \tag{6}$$

$$f_{outer} = (1 - \varepsilon) f_{sigm}(x; a_{outer}, c_{outer}) + \varepsilon \tag{7}$$

$$f_{CP} = (1 - \varepsilon) f_{sigm}(x; a_{CP}, c_{CP}) + \varepsilon \tag{8}$$

where the parameters $\alpha$ and $c$ for each component are given in Table 1 and $\varepsilon$ is a small positive factor defined by 0.05.

### 2.1.5. Segmentation of lumen, outer wall and CP

In this step, an extension of the active contour models [24] is implemented for the lumen, the outer wall and the CP segmentation. The main idea of active contour models is to evolve a curve, aiming to detect different objects in a 2D image by representing the interface of

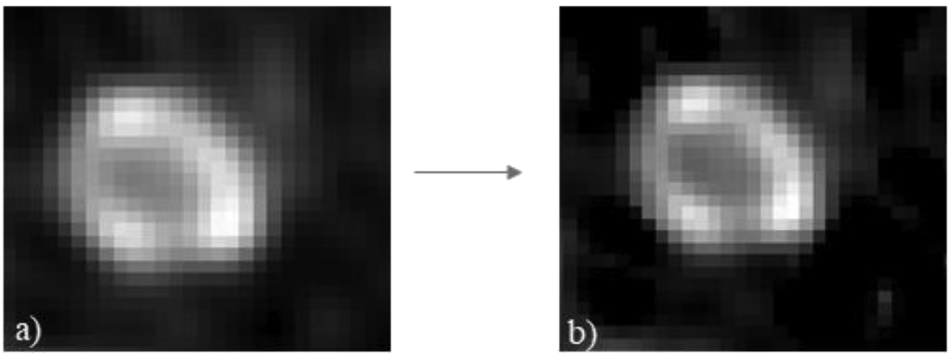


**Fig. 2.** Blooming effect removal.

**Table 1**
The utilized parameters for the lumen, outer wall and CP.

| Parameters | $a$ | $c$ |
|---|---|---|
| Lumen | $a_{1,lumen} = 0.02 a_{2,lumen} = -0.01$ | $c_{1,lumen} = min([max([\bar{I}_{lumen} - l_{thres} \quad 150]) \quad 150]) c_{2,lumen} = \bar{I}_{lumen} + cp_{thres}$ |
| Outer wall | $a_{outer} = 0.02$ | $c_{outer} = min(200 \quad max([\bar{I}_{lumen} - l_{thres} - ncp_{thres} \quad 100]))$ |
| CP | $a_{CP} = 0.05$ | $c_{CP} = \bar{I}_{lumen} + cp_{thres}$ |

the surface using a higher dimensional function, the level set function. In this way, the utilized level set function is represented as a 3D function, incorporating the additional input parameter $t$, which represents the time. In our approach, the detected curve is represented using the zero level set of a Lipschitz function:

$$C = d\omega = \{(x, y, t) \in \Omega: \phi(x, y, t) = 0\} \quad (9)$$

$$inside(C) = \omega = \{(x, y, t) \in \Omega: \phi(x, y, t) > 0\} \quad (10)$$

$$outside(C) = \omega = \{(x, y, t) \in \Omega: \phi(x, y, t) < 0\}, \quad (11)$$

where $x$, $y$are the spatial coordinates of the 2D CTCA image and $t$is the time.

We improved the implementation of the level set segmentation approach by incorporating a prior shape to allow an object segmentation with a similar given prior shape [25]. The prior shape for the coronary arterial inner wall detection is defined as a tubular mask across the vessel centerline with a small radius, whereas the prior shape for the outer wall segmentation is defined as the segmented inner wall mask.

As far as the 2D segmentation procedure is concerned, the process includes four stages: (i) the update of the lumen intensities, (ii) the estimation of an initial binary image, (iii) the calculation of the curve speed function and, (iv) the sparse field algorithm implementation. More specifically, we update the lumen membership function, taking into consideration only a small region of the CTCA image. The pixels of this region are defined as those whose Euclidean distance transform from the extracted vessel centerline is lower than the quotient of the lumen radius with the pixel spacing parameter of the CTCA image. Consequently, an initial binary image ($\phi$) is required to implement the level set based segmentation approach. This initial binary image is approximated, based on the hypothesis that when the updated lumen membership function multiplied with a threshold value is larger than 500 HU, the pixels of the initial image are ones, otherwise the pixels are zeros. A shape function $\psi$ and a labelling function $L$ are also estimated to define the utilized speed function. The estimated speed function is based on the Chan et al. approach [24] and is given as:

$$E(\phi, \psi, L) = E_{cv} + E_{shape} + E_{\psi} \quad (12)$$

where $E_{cv}$is the Chan-Vese energy [29], $E_{shape}$ is the shape comparison term and $E_{\psi}$ is the labelling function, which is used to indicate the regions in which shape priors should be enforced. The segmentation procedure is continuing by the implementation of the sparse field algorithm, proposed by Whitaker et al. [26], aiming to minimize the representation of $\phi(x, y)$ ($\phi(x, y) \approx 0$) and to represent accurately the curve. The sparse field algorithm is implemented twice to achieve a smooth 2D lumen segmentation. The same segmentation procedure is applied for the outer wall segmentation, updating in this case the previously estimated outer wall membership function.

As far as the CP segmentation is concerned, the procedure is similar with the aforementioned ones. However, it is implemented only in the region of interest (ROI), which is inside the outer wall and outside the inner wall of the coronary vessel. Due to the smaller number of pixels of the CP segmented mask, the sparse field algorithm is implemented once in this case.

#### 2.1.6. Segmentation of NCP

Contrary to the CP, the NCP has a lower intensity, that makes the detection of the NCP a challenging problem. An indicative study has proved that the luminal intensity is clearly related to the intensity inside the atherosclerotic plaque. Thus, in this study due to the lower intensities of NCP, the NCP cannot be successfully identified by a level set approach, since the intensity ranges are close to the intensity ranges of the outer wall. The identification of NCP is achieved by a dynamic thresholding technique. Thresholding is a conventional segmentation technique, in which the image pixels are partitioned depending on their intensity value, using an appropriate threshold value. However, in the case of dynamic thresholding segmentation, the threshold value is not constant and relies on the mean intensities values of pixels, which correspond to the lumen region.

The main idea of this approach is to define the intensity range of the dynamic threshold technique around the luminal intensity and the range of NCP HU values is extracted based on the mean luminal intensity (*ml)*. The *ml* is computed after the implementation of the Frangi vesselness filter. The *ml* value is the mean value of the highest of half image intensities, which are higher than 100 HU, considering only the parts of the CTCA image, which are potential coronary vessels. After the definition of the *ml,* the range of NCP pixels intensities is defined from 100 HU to the *ml* value. In addition to this, the aforementioned segmentation approach is implemented in the ROI, which is located between the segmented outer wall and lumen.

In Fig. 3, we demonstrate different examples of the segmentation of the lumen, CP and NCP.

#### 2.1.7. 3D surface reconstruction

The Marching cubes algorithm, which has been proposed by Lorensen and Cline [27], is applied to construct the 3D surfaces for the inner and the outer wall, the CP and the NCP. More specifically, a triangle topology is defined by constant density surfaces, applying the divide- and- conquer approach to create inter-slice connectivity.

### 2.2. Dataset

#### 2.2.1. Dataset to compare with VH-IVUS modality

The proposed methodology was validated using imaging data from 18 patients, who underwent coronary angiography, IVUS and CTCA imaging for clinical purposes. All of the patients enrolled in the study had a significant luminal stenosis (> 50%), which was initially confirmed by the CTCA imaging and further investigated by VH-IVUS. This imaging dataset was provided by the Heart Institute, University of Sao Paulo, São Paulo, Brazil and the CTCA images acquisition was performed using a 64slice MDCT scanner (Aquillion 64TM, Toshiba Medical Systems, Japan), while the IVUS examination was performed using a 20 MHz electronic multi-array 2.9 F catheter (Eagle Eye®, Volcano Corporation Inc) connected to a dedicated console (InVision Gold®, Volcano Corporation Inc., San Diego, CA, USA).

#### 2.2.2. Dataset to compare with manual expert's annotations

The imaging data were acquired from 27 patients, who underwent CTCA imaging for clinical purposes and one of their coronary arteries was selected for manual expert's analysis. 8 coronary arteries had no significant stenosis (< 30%), 8 had an intermediate stenosis (30%–50%), 8 had a significant stenosis (50%–70%) and 3 coronary arteries were fully occluded with a stenosis higher than 70%. In addition to this, the utilized imaging dataset was derived by six different

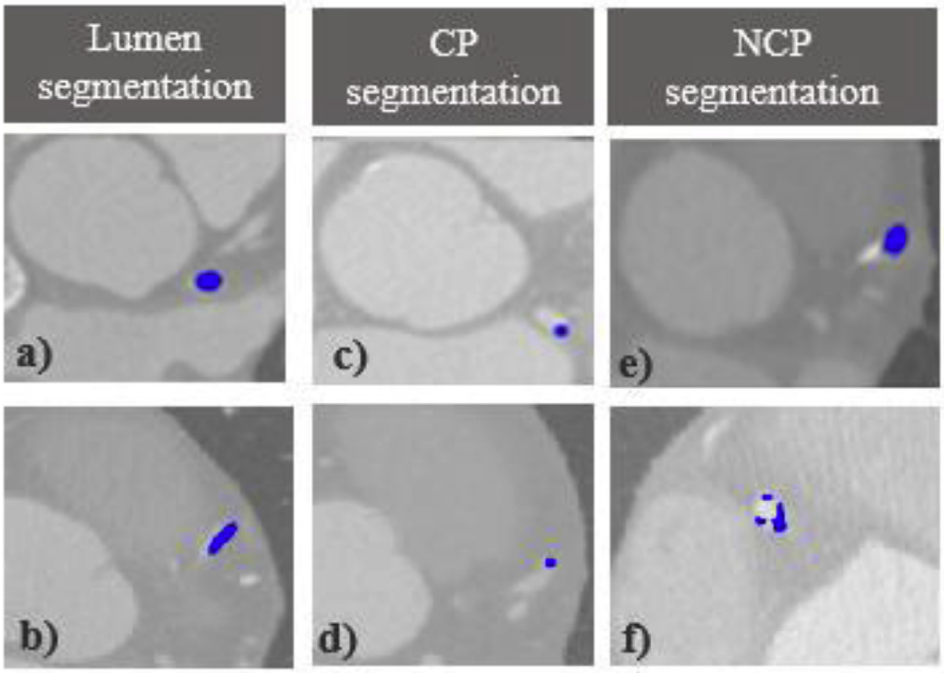


**Fig. 3.** Lumen (a,b), CP (c,d) and NCP (e,f) segmentation.

medical centers and the coronary arteries were scanned with different CTCA scanners (64-slice Dual Source Siemens SOMATOM Definition Flash® CT scanner, Philips Brilliance 64 CT Scanner®, 64-slice General Electric Medical Systems Discovery PET/CT 690®).

### 2.3. Validation approach

The proposed methodology was validated using two different approaches, which were based on different type of imaging data and different datasets. The first validation approach was dedicated to the identification of CP and NCP, utilizing VH-IVUS frames and all the utilized arteries were pathological and had a significant degree of stenosis On the other hand, the second validation approach aimed to compare the pixel by pixel segmentation procedure, as far as the lumen, CP and NCP pixels are concerned, in both pathological and non-pathological conditions, where the CTCA images derive by different CTCA scanners.

#### 2.3.1. CTCA vs VH-IVUS comparison

The proposed methodology was validated using the corresponding VH-IVUS frames. VH-IVUS frames analysis was implemented based on a study introduced by Bourantas et al. [28]. The registration between the CTCA and VH-IVUS imaging was achieved using specific anatomical landmarks, such as characteristic calcifications, stents, side-branches, and additionally the co-registration procedure was validated by measuring the distances between the select fiducial anatomical landmarks and the coronary ostium.

In this validation approach, three different comparison metrics were used: (a) the atherosclerotic plaque volume ($mm^3$) and (b) the atherosclerotic plaque length of lesion (mm), which were based on the extracted 3D coronary artery model, and (c) the atherosclerotic plaque area ($mm^2$), which was based on the 2D CTCA and VH-IVUS frames analysis. In our study, the soft atherosclerotic plaques (NCP lesion) was considered as the total of three different subtypes of atherosclerotic plaques, the fibrous, the fibrofatty and the necrotic core tissue.

#### 2.3.2. CTCA manual expert's annotations comparison

A medical expert, who was blind to the contours generated by the automated segmentation algorithm, manually annotated pixel by pixel the lumen, the CP and the NCP pixels, when existed, in 1350 CTCA slices and the comparison procedure was performed in each annotated 2D CTCA slice. In addition to this, the utilized comparison metrics were the DICE coefficient and the Hausdorff Distance (HD).

## 3. Results

### 3.1. Comparison with VH-IVUS

In the validation procedure, 18 coronary arteries and 90 CTCA and VH-IVUS slices were identified, registered and used for the validation procedure. After the implementation of the proposed methodology and the analysis of VH-IVUS slices, we identified 6 CP lesions and 12 NCP lesions and all the lesions detected by VH-IVUS modality can also be detected by the proposed segmentation algorithm.

The correlation between CTCA and VH-IVUS is demonstrated using Bland Altman analysis and linear regression correlation analysis. The Bland Altman plots and the correlation plots are shown in Fig. 4 for the CP volume and CP length of lesion, whereas in Fig. 5, the corresponding plots for the NCP volume and length of the lesion are shown. As far as the 2D comparison procedure is concerned, in Fig. 6 and Fig. 7 the Bland Altman analysis and the correlation plot for the CP area and NCP area are shown, respectively. Although CP pixels can be easily identified using CTCA modality, we observe in the Bland Altman analysis plot in Fig. 6 that for the low area of CP there is an underestimation of CP with CTCA, whereas for the high area of CP there is an overestimation of CP with CTCA. The comparison results indicate that the Pearson's correlation ($r$) for the CP volume, the length of the lesion and the area was 0.93, 0.84 and 0.85, while the Degree of correlation ($R^2$) was 0.85, 0.71 and 0.72, for the CP volume, the CP length of the lesion and the CP area, respectively.

The corresponding correlation values of NCP are 0.92, 0.95 and 0.81 for Pearson's correlation ($r$), and 0.85, 0.9, 0.64 for the Degree of correlation ($R^2$), for the plaque volume, the length of lesion and the area, respectively. The mean values of the plaque volume extracted by the proposed methodology are $6.98 \pm 4.59\,mm^3$ and $120.59 \pm 83.11\,mm^3$ for CP and NCP, respectively, whereas the

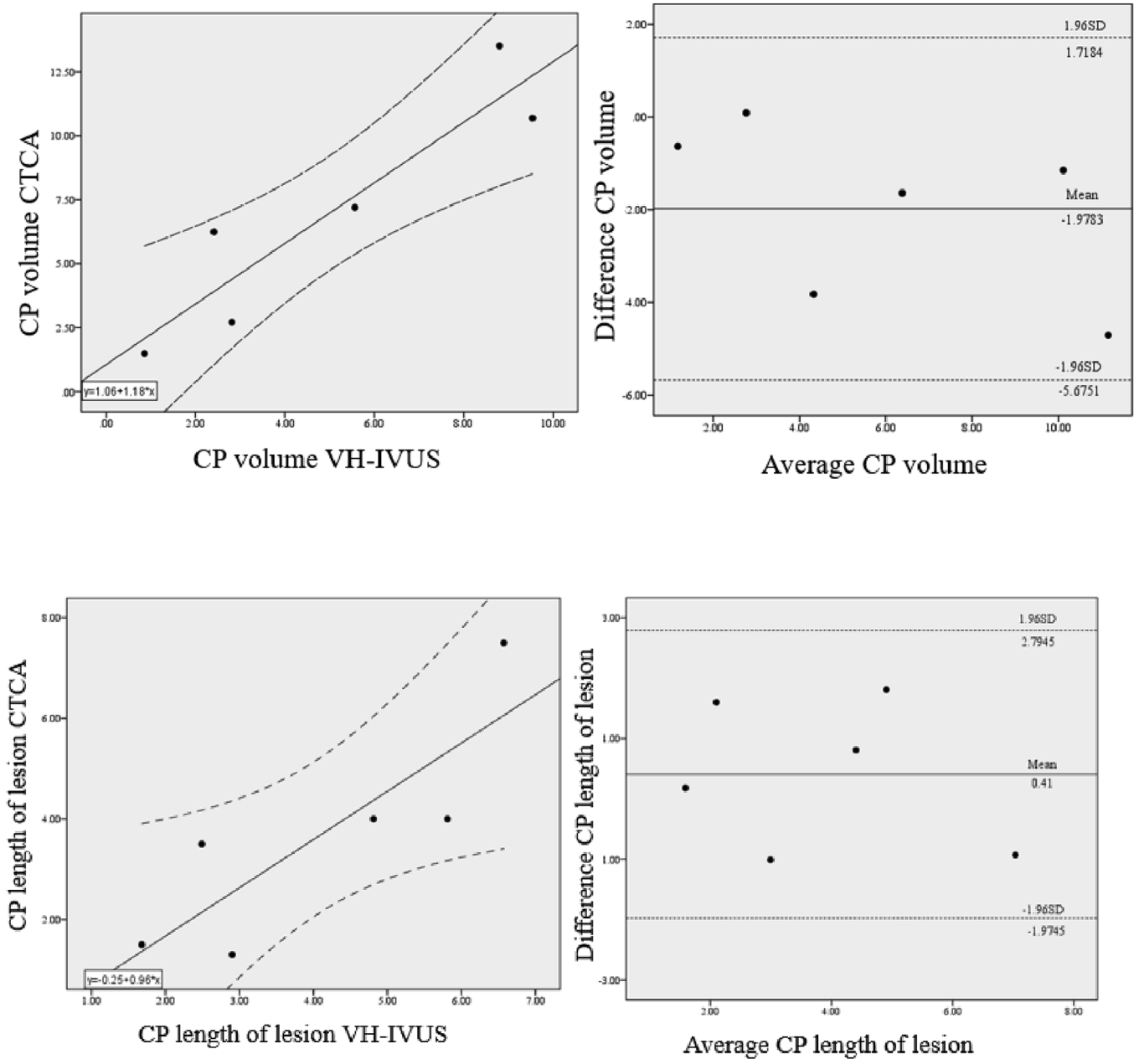


**Fig. 4.** Bland-Altman and correlation plots for CTCA and VH-IVUS for the CP volume and the CP length of lesion.

corresponding mean values of the plaque volume by VH-IVUS are $5 \pm 3.58\,mm^3$ for CP and $129.28 \pm 101.3\,mm^3$ for NCP. The mean value of the CP length of the lesion is $3.63 \pm 2.25$ mm and for the NCP lesion is $40.375 \pm 18.62$ mm, while the mean value of the CP length of lesion based on VH-IVUS is $4.04 \pm 1.97$ mm and of NCP lesion $46 \pm 18.29$ mm. In addition to this, the mean value of the plaque area based on CTCA and VH-IVUS is $0.59 \pm 0.99\,mm^2$ and $0.42 \pm 0.61\,mm^2$ for CP, respectively, and $2.31 \pm 1.17\,mm^2$ and $2.26 \pm 1.38\,mm^2$ for NCP, respectively. The previously described correlation metrics and the mean values of the validation metrics are shown in Table 2.

### 3.2. Comparison with manual annotations

The utilized data were acquired from 27 patients, who underwent CTCA imaging for clinical purposes. 1350 CTCA slices were utilized and manually annotated for the lumen segmentation validation, whereas 78 CTCA slices and 47 CTCA slices were utilized for the CP and NCP segmentation validation procedure, respectively. In Table 3, we present the DICE and HD for the lumen segmentation, whereas in Table 4 and Table 5, we present the DICE and HD distributions for the CP and NCP, respectively. The mean value of DICE coefficient was $0.72 \pm 0.08$, $0.7 \pm 0.09$ and $0.62 \pm 0.07$, for the lumen, CP and NCP, respectively, whereas the mean HD value was $1.95 \pm 0.45$, $1.74 \pm 0.34$ and $1.95 \pm 0.36$ for lumen, CP and NCP, respectively. In Fig. 8, we show the manual and the automated segmentation for the lumen, the CP and the NCP.

## 4. Discussion

This work presents an automated methodology for the reconstruction of the lumen, the outer wall, the CP and the NCP of coronary arteries based on CTCA images. The proposed study constitutes a novel approach due to its automated nature to identify the lumen, the outer

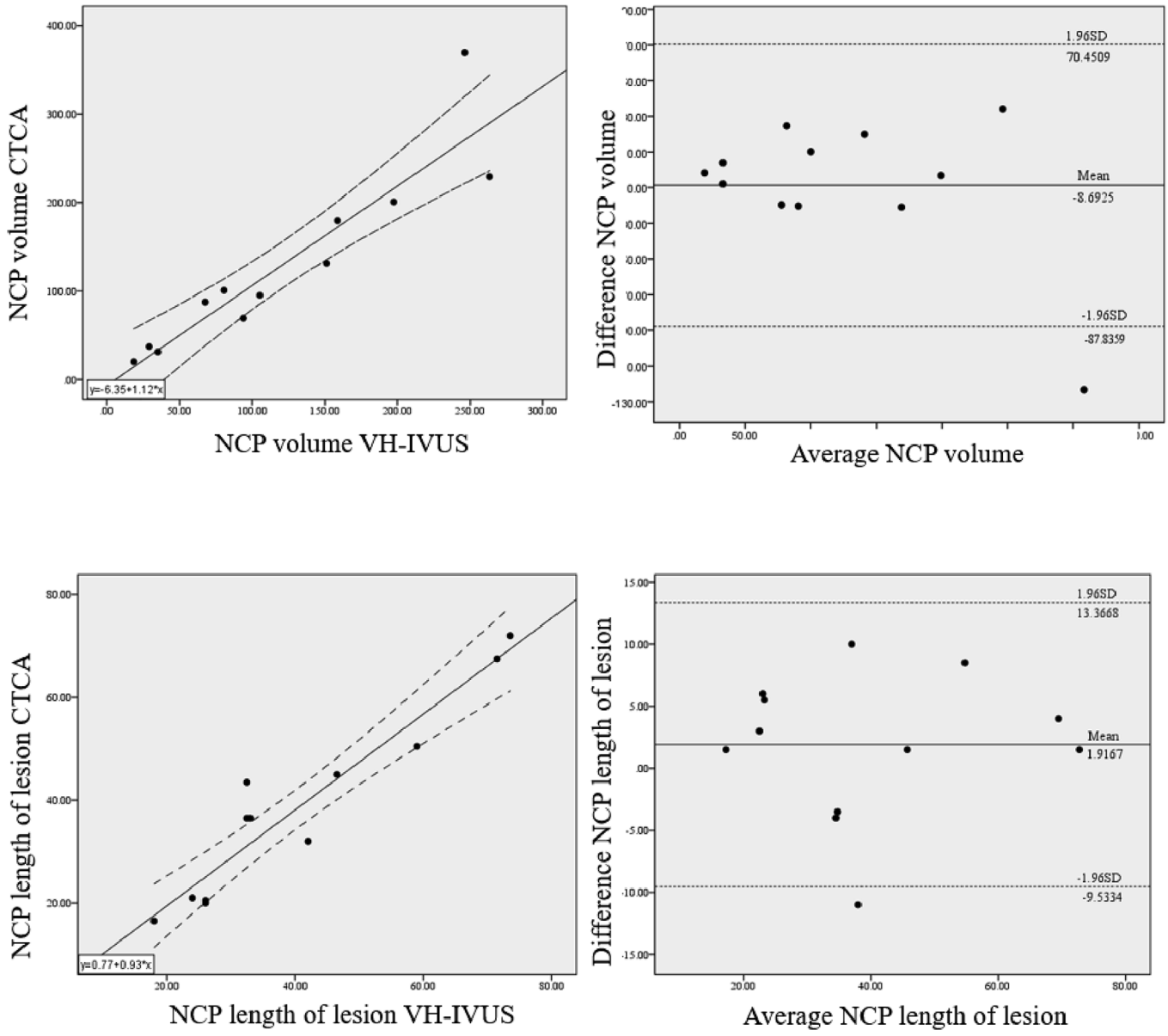


**Fig. 5.** Bland-Altman and correlation plots for CTCA and VH-IVUS for the NCP volume and NCP length of lesion.

wall (plaque burden region), the CP and NCP. The accuracy of the proposed methodology is evaluated based on the VH-IVUS modality, which with IVUS modality constitute well established modalities for the validation of CTCA image analysis techniques, while it is also validated in terms of the lumen, CP and NCP segmentation accuracy, by directly comparing medical doctor's annotations. To our knowledge, the validation approach of CP and NCP segmentation constitutes the novelty of the study, since existing in the literature studies are dedicated either on the automated plaque segmentation in comparison with IVUS and VH-IVUS modality [6,7,10] or manual plaque detection in comparison with IVUS and VH-IVUS modality [5,8].

As far as the CP is concerned, its pixels can be easily identified using the CTCA modality due to their high intensity values. On the other hand, the detection of NCP constitutes a challenging problem, since the NCP intensity is characterized by lower intensity values, close to the perivascular fat tissue [29]. The CTCA modality is a promising non-invasive technique to accurately detect the NCP in the plaque burden. Direct identification and quantification of NCP and plaque burden is an important issue, since the NCP has been indicated as a significant indicator of acute coronary syndromes [30] and its presence is more likely to be associated with high-risk groups, such as those with elevated inflammatory biomarkers and those suffering from diabetes mellitus [31,32].

In the proposed methodology, two 2D segmentation approaches are implemented for the detection of CP and NCP. Both the CP and the NCP detection requires the estimation of heuristic parameters, which are based on the intensity threshold values defined in the literature and not tuned based on the validation dataset. The identification of CP relies on level set models, whereas the NCP detection is based on a dynamic thresholding technique. Although the level set models achieve an accurate segmentation, in the case of NCP this is not applicable, since the HU intensities of NCP proposed in the literature are close to those of the outer wall. In addition to this, the performance of the proposed methodology to identify the lumen and the outer wall has already been validated in a recently published study [33], using both manual expert's annotations on CTCA images and IVUS images analysis. Therefore, a validated region of interest detection ensures the accurate CP and NCP detection. As a result, a good correlation was indicated and no significant differences of plaque volumes, lengths of coronary lesions and areas quantified by CTCA and VH-IVUS were observed. In Table 6, a

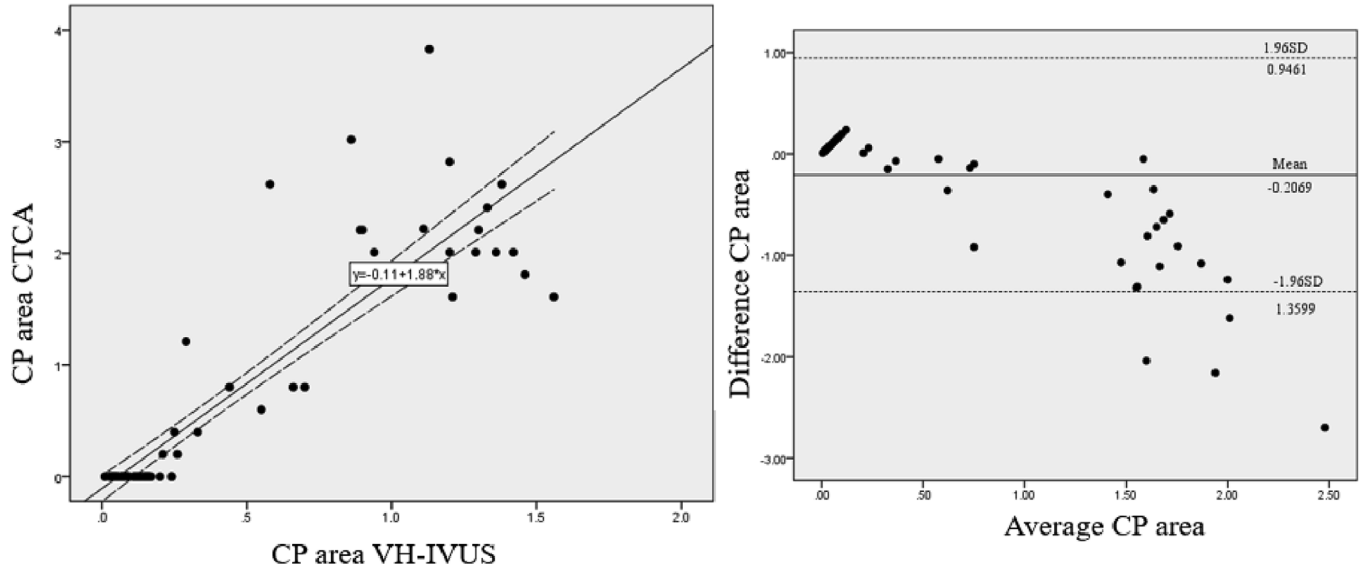


**Fig. 6.** Bland-Altman and correlation plots for CTCA and VH-IVUS for the CP area.

comparison of the NCP volumes derived by the proposed methodology and by other methodologies is presented. It is observed that the study proposed by Dey et al. [6] indicate a higher correlation. This study is concentrated only on the quantification and detection of NCP and does not provide any details about the vessel geometry and the distribution of the plaque in 3D space. In addition to this, the study proposed by Dey et al. requires by the user the starting and the ending point of the plaque lesion to quantify the NCP lesion. Contrary to this study, our proposed methodology is able to identify either CP or NCP lesions in the entire coronary arterial tree, indicating only the starting point of the coronary bifurcation and the ending points of each coronary artery branch.

In addition to this, different studies have been proposed in the literature for the CP and NCP detection which rely either on a specific HU threshold analysis [5,6,10] or on manual CP and NCP detection [8,9], concluding that the proposed approach outperforms the existing in the literature studies, since no manual interaction is required and it is fully adapted on each CTCA image quality.

Furthermore, several studies have been conducted focusing on the ability of expert observers to detect and annotate manually NCP using CTCA. These studies indicate a strong correlation with the NCP volumes derived by IVUS. However, these approaches are time consuming, since they are not implemented in an automatic or semi-automatic manner [9,34,35]. In our methodology, this limitation is overcome, since the proposed methodology requires low computation time for the 3D reconstruction of coronary arteries. In addition to this, it should be noted that the proposed methodology achieves an expedite 3D coronary reconstruction of the entire coronary arterial tree. In this way, the atherosclerotic plaque can be identified not only in coronary segments, but also in crucial regions, such as the coronary bifurcations.

Except from the studies for the identification of CP and NCP, several studies presented in the literature aimed to analyze CTCA images and detect the inner wall vessel boundaries, taking advantage of different methodological solutions. More specifically, a localized region-based level set framework was utilized by Wang et al. [36] to provide the inner wall of coronary artery main branches, whereas Bouraoui et al. [37] developed an automated methodology for the coronary artery inner wall segmentation, employing mathematical morphology techniques and discrete geometrical tools. In a different attempt, Shahzad et al. [38] proposed a methodology to automatically detect and quantify coronary artery stenosis employing a kernel regression model, while Chen et al. [39] proposed a discrete wavelet transformation (DWT) based methodology for the automated segmentation of coronary

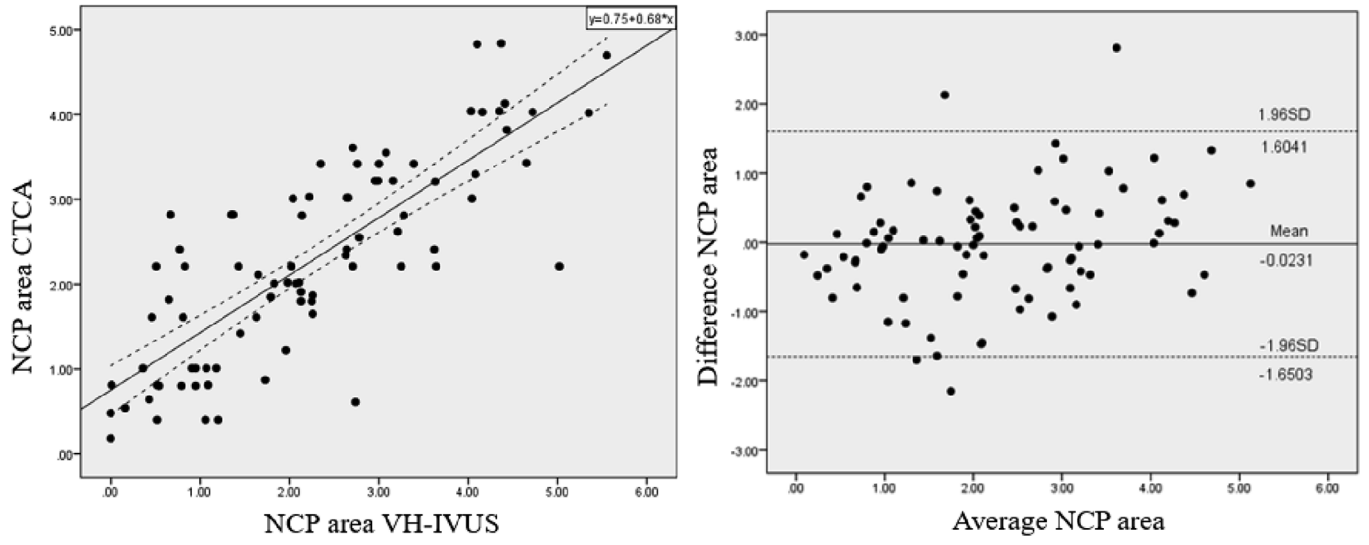


**Fig. 7.** Bland-Altman and correlation plots for CTCA and VH-IVUS for the NCP area.

**Table 2**
CTCA and VH-IVUS validation metrics.

| | Metrics | CTCA | VH-IVUS | Pearson's correlation ($r$) | Degree of correlation ($R^2$) | p-value |
|---|---|---|---|---|---|---|
| Calcified Plaques | volume | 6.98 ± 4.59 | 5 ± 3.58 | 0.93 | 0.85 | < 0.001 |
| | length of lesion | 3.63 ± 2.25 | 4.04 ± 1.97 | 0.84 | 0.71 | < 0.001 |
| | area | 0.59 ± 0.99 | 0.42 ± 0.61 | 0.85 | 0.72 | < 0.001 |
| Noncalcified Plaques | volume | 120.59 ± 83.11 | 129.28 ± 101.3 | 0.92 | 0.85 | < 0.001 |
| | length of lesion | 40.375 ± 18.62 | 38.46 ± 18.29 | 0.95 | 0.90 | < 0.001 |
| | area | 2.31 ± 1.17 | 2.26 ± 1.38 | 0.81 | 0.64 | < 0.001 |

**Table 3**
Validation metrics against manual annotations for the lumen segmentation.

| Cases | Lumen | | Cases | Lumen | |
|---|---|---|---|---|---|
| | DICE | HD | | DICE | HD |
| **#1** | 0.79 ± 0.1 | 2.39 ± 0.86 | **#15** | 0.77 ± 0.05 | 2.43 ± 0.18 |
| **#2** | 0.83 ± 0.05 | 2.07 ± 0.35 | **#16** | 0.66 ± 0.14 | 1.6 ± 0.43 |
| **#3** | 0.67 ± 0.09 | 1.69 ± 0.57 | **#17** | 0.52 ± 0.12 | 1.78 ± 0.58 |
| **#4** | 0.8 ± 0.06 | 1.77 ± 0.55 | **#18** | 0.68 ± 0.08 | 1.588 ± 0.73 |
| **#5** | 0.79 ± 0.04 | 1.63 ± 0.3 | **#19** | 0.81 ± 0.1 | 1.86 ± 0.66 |
| **#6** | 0.72 ± 0.1 | 2.09 ± 0.37 | **#20** | 0.77 ± 0.08 | 1.68 ± 0.43 |
| **#7** | 0.64 ± 0.12 | 1.54 ± 0.16 | **#21** | 0.58 ± 0.13 | 2.03 ± 0.34 |
| **#8** | 0.75 ± 0.07 | 2.22 ± 0.28 | **#22** | 0.68 ± 0.12 | 1.9 ± 0.57 |
| **#9** | 0.65 ± 0.09 | 2 ± 0.31 | **#23** | 0.59 ± 0.1 | 2.04 ± 0.73 |
| **#10** | 0.66 ± 0.07 | 2.3 ± 0.17 | **#24** | 0.78 ± 0.07 | 1.64 ± 0.34 |
| **#11** | 0.64 ± 0.03 | 2.31 ± 0.38 | **#25** | 0.73 ± 0.09 | 1.84 ± 0.44 |
| **#12** | 0.73 ± 0.06 | 2.9 ± 0.97 | **#26** | 0.82 ± 0.05 | 2.05 ± 0.32 |
| **#13** | 0.65 ± 0.03 | 2.24 ± 0.4 | **#27** | 0.8 ± 0.08 | 1.67 ± 0.62 |
| **#14** | 0.81 ± 0.07 | 1.43 ± 0.23 | | | |

**Table 4**
Validation metrics against manual annotations for the calcified plaques segmentation.

| Cases | Calcified Plaques | |
|---|---|---|
| | DICE | HD |
| #1 | 0.79 ± 0.12 | 1.33 ± 0.16 |
| #2 | 0.66 ± 0.11 | 2.38 ± 0.27 |
| #3 | 0.67 ± 0.09 | 2.56 ± 0.23 |
| #4 | 0.62 ± 0.13 | 1.27 ± 0.24 |
| #5 | 0.61 ± 0.15 | 1.89 ± 0.38 |
| #6 | 0.62 ± 0.06 | 1.82 ± 0.58 |
| #7 | 0.72 ± 0.07 | 1.58 ± 0.36 |
| #8 | 0.71 ± 0.05 | 1.31 ± 0.21 |
| #9 | 0.78 ± 0.04 | 1.94 ± 0.51 |
| #10 | 0.68 ± 0.07 | 1.61 ± 0.63 |
| #11 | 0.72 ± 0.08 | 1.87 ± 0.32 |
| #12 | 0.73 ± 0.17 | 1.35 ± 0.43 |
| **#13** | 0.76 ± 0.09 | 1.82 ± 0.15 |

**Table 5**
Validation metrics against manual annotations for the non-calcified plaques segmentation.

| Cases | Non-calcified Plaques | |
|---|---|---|
| | DICE | HD |
| #1 | 0.69 ± 0.08 | 2.39 ± 0.56 |
| #2 | 0.65 | 1.41 |
| #3 | 0.78 ± 0.06 | 1.42 ± 0.2 |
| #4 | 0.51 ± 0.09 | 2.98 ± 0.34 |
| #5 | 0.54 ± 0.08 | 1.28 ± 0.38 |
| #6 | 0.65 ± 0.08 | 2.25 ± 0.46 |
| #7 | 0.49 ± 0.08 | 1.89 ± 0.56 |

arteries in CTCA image datasets. In the same rationale, Chen et al. [40] applied primarily a region growing algorithm for the initial coronary arteries detection and then a vessel-texture discrimination algorithm was implemented for the precise coronary vessel segmentation. In the same direction, an active contour framework with accurate shape and size constraints on the vessel cross-sectional planes was utilized by Cheng et al. [41] to provide the vessel segmentation using 3D CTCA data. Kitamura et al. [42] and Athanasiou et al. [43] presented novel methodologies for both the coronary lumen and calcified plaques segmentation, based on multi-label graph cuts and Gaussian Mixture Model, respectively.

These studies aimed basically to segment automatically the inner wall of the coronary arteries and are evaluated at the level of 2D segmentation and do not provide details about the 3D geometry of the coronary arteries, whereas some of them are only dedicated to detect and quantify the coronary artery stenosis. Moreover, the proposed in the literature studies which incorporate image processing techniques are not capable of identifying either the plaque burden region or detect and characterize the atherosclerotic plaque. As far as the implemented methodology is concerned, our proposed methodology incorporates a 3D level set approach with a prior shape for the lumen, the outer wall and the CP and utilizes an innovative combination of energy function. To our knowledge, this type of approach for the segmentation of the full arterial coronary tree constitutes a novel aspect.

Other studies have demonstrated that the mean luminal attenuation value varies, due to the implementation of different acquisition dose protocols. In addition to this, it has been indicated that the intra-arterial injection of iodinated contrast agent affects not only the luminal attenuation value, but also the atherosclerotic plaque attenuation value [44]. In our study, the segmentation of NCP is clearly related to the mean luminal attenuation and more specifically the computed *ml* value varies from 276 to 418 HU. This means that the proposed methodology can be adapted either on different acquisition protocols or on different CTCA image quality, since the *ml* value respects to different HU intensity values. In addition to this, the proposed segmentation algorithm can be applied either on high or low dose acquisition protocols, since the utilized membership functions are totally adapted in the *ml* value, which in case of low dose acquisition protocol is much lower. Moreover, as far as the optimization of these parameters is concerned, the proposed methodology is incorporated in a software tool and the parameters could be optimized according to a calibration procedure. More specifically, an expert user can annotate some pixels for each component (inner wall, outer wall, calcified plaques, noncalcified plaques) and an accurate threshold is estimated for each component. Thus, although the calibration procedure requires an expert user and needs more time complexity, the membership functions are more adapted on each CTCA image.

Apart from the selected HU threshold values for NCP, another important factor for the accurate identification of NCP is the reliable identification of ROI. Accurate lumen and outer wall area segmentation results in accurate plaque burden region detection. In our study, the detection of the ROI has already been validated [33] using both manual expert's annotations and a 3D reconstruction methodology using angiographic data fuzzed with IVUS data [28]. Thus, the presented methodology for NCP detection is a promising technique allowing the accurate plaque burden characterization.

Furthermore, it should be noted that the VH-IVUS permits the plaque characterization with a higher spatial resolution than the non-

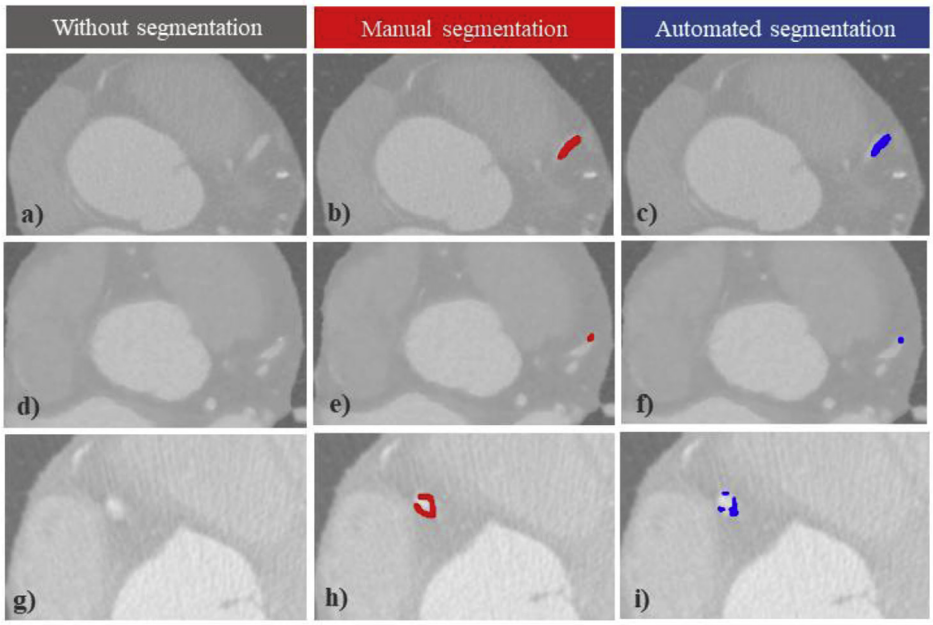


**Fig. 8.** Without segmentation, manual and automated segmentation for the lumen (a, b, c), for the CP (d, e, f) and the NCP (g, h, i), respectively.

invasive CTCA. Due to its low spatial resolution, CTCA is limited to identify the different subtypes of the NCP, contrary to VH-IVUS and to extract in a reliable manner the smaller atherosclerotic plaque volumes. This approach was validated using large NCP volumes, ranging from 18.39 to 263.38 $mm^3$, which are more prone to rupture.

Moreover, the presented methodology incorporates the blooming effect removal, aiming to improve the CTCA image visualization of calcifications. In this manner, an accurate 3D quantification of CP is achieved, without overestimating the CP volume, which results in the overestimation of the coronary lumen stenosis. The blooming effect remains a challenging artifact of CTCA images, which can be limited by deconvolution and filtering techniques. In addition to this, we implement a deconvolution procedure on the high intensity image's pixels to quantify in a reliable manner the CP volume. Thus, no significance difference is observed between the CP volumes derived by the presented methodology and those extracted by VH-IVUS analysis, achieving a high Pearson's correlation ($r = 0.93$).

## 5. Limitations

Although the proposed methodology provides promising results for the reconstruction of the entire coronary arterial tree and provides an accurate distribution of the CP and NCP in the 3D space, a limitation of this study is the small number of the 3D CP, as far as the comparison against VH-IVUS is concerned.

Another limitation of the proposed study is the calculation of the atherosclerotic plaque volume based on the VH-IVUS images analysis. More specifically, the calculation approach is based on atherosclerotic plaque area cross-section multiplied with the number of slices and the slice thickness, which is a well established methodology, reported in different already existing studies [45]. However, this volumetric quantification approach has not been endorsed by the Quantitative Imaging Biomarkers Alliance (QIBA).

In addition to this, another significant aspect of the IVUS modality use is that IVUS modality does not accurately quantify the densely CP, because plaque boundaries are located into the acoustic shadow, which is considered a basic limitation of IVUS use in the quantification of CP. Nevertheless, in this study CP detection is validated against VH-IVUS modality, which constructs tissue maps that classify plaque into four major tissue types (fibrous, fibro-fatty, necrotic core, and dense calcium).

## 6. Conclusions

In this work, we present an efficient methodology for the detection of CP and NCP from CTCA using active contour models and dynamic threshold technique, respectively. The innovative aspect of the proposed methodology is the provision of accurate 3D models for the CP and NCP, taking into consideration the vessel curvature, allowing the assessment of the atherosclerotic plaque distribution in the 3D space. The identification of both types of atherosclerotic plaques utilizing a non-invasive cardiovascular imaging modality, may be considered as a significant step towards the diagnosis and management of CAD. Undoubtedly, different segmentation techniques might lead to a different coronary artery 3D reconstruction. Thus, the selection and implementation of an accurate CTCA segmentation technique may result in an accurate coronary artery 3D model, which may contribute to a reliable quantification and evaluation of coronary artery stenosis and to the investigation of its biomechanical features, as well. More specifically, the utilization of the reconstructed geometries for computational modelling of blood flow or the accumulation of lipids [46,47] in the arterial wall can improve the decision making of cardiologists for the

**Table 6**
Comparison of the proposed methodology with the other methodologies for the NCP detection.

| Study | Volume by CTCA | Volume by IVUS | Pearson's correlation ($r$) | Degree of correlation ($R^2$) | Sample size |
|---|---|---|---|---|---|
| Brodoefel et al. [7] | 56.7 ± 30 | 55.8 ± 26 | – | 0.84 | 14 |
| Dey et al. [6] | 116 ± 80.1 | 105.9 ± 83.5 | 0.94 | – | 22 |
| Leber et al. [8] | 59.8 ± 76.6 | 67.7 ± 67.9 | – | 0.69 | 65 cross-sections |
| Proposed methodology | 120.59 ± 83.11 | 129.28 ± 101.3 | 0.92 | 0.85 | 12 plaques, 47 cross sections |

management of CAD.

## Acknowledgements

This work is partially funded by the European Commission: Project SMARTOOL, “Simulation Modeling of coronary ARTery disease: a tool for clinical decision support —SMARTool”, GA number: 689068. This manuscript reflects only the authors' view. The Commission is not responsible for any use that may be made of the information it contains.

## References

[1] W. H. O. (WHO), The atlas of heart disease and stroke, Available: http://www.who.int/cardiovascular_diseases/en/cvd_atlas_16_death_from_stroke.pdf.
[2] J. Eckert, M. Schmidt, A. Magedanz, T. Voigtländer, A. Schmermund, Coronary CT angiography in managing atherosclerosis, Int. J. Mol. Sci. 16 (2015) 3740–3756.
[3] S.B. Puchner, T. Liu, T. Mayrhofer, Q.A. Truong, H. Lee, J.L. Fleg, et al., High-risk plaque detected on coronary CT angiography predicts acute coronary syndromes independent of significant stenosis in acute chest pain: results from the ROMICAT-II trial, J. Am. Coll. Cardiol. 64 (2014) 684–692.
[4] K. Patel, J. Tarkin, P.W. Serruys, E. Tenekecioglu, N. Foin, Y.-J. Zhang, et al., Invasive or non-invasive imaging for detecting high-risk coronary lesions? Expert Rev. Cardiovasc. Ther. 15 (2017) 165–179.
[5] S. Voros, S. Rinehart, Z. Qian, G. Vazquez, H. Anderson, L. Murrieta, et al., Prospective validation of standardized, 3-dimensional, quantitative coronary computed tomographic plaque measurements using radiofrequency backscatter intravascular ultrasound as reference standard in intermediate coronary arterial lesions: results from the ATLANTA (assessment of tissue characteristics, lesion morphology, and hemodynamics by angiography with fractional flow reserve, intravascular ultrasound and virtual histology, and noninvasive computed tomography in atherosclerotic plaques) I study, JACC Cardiovasc. Interv. 4 (2011) 198–208.
[6] D. Dey, T. Schepis, M. Marwan, P.J. Slomka, D.S. Berman, S. Achenbach, Automated three-dimensional quantification of noncalcified coronary plaque from coronary CT angiography: comparison with intravascular US, Radiology 257 (2010) 516–522.
[7] H. Brodoefel, C. Burgstahler, M. Heuschmid, A. Reimann, F. Khosa, A. Kopp, et al., Accuracy of dual-source CT in the characterisation of non-calcified plaque: use of a colour-coded analysis compared with virtual histology intravascular ultrasound, Br. J. Radiol. 82 (2009) 805–812.
[8] A.W. Leber, A. Becker, A. Knez, F. von Ziegler, M. Sirol, K. Nikolaou, et al., Accuracy of 64-slice computed tomography to classify and quantify plaque volumes in the proximal coronary system: a comparative study using intravascular ultrasound, J. Am. Coll. Cardiol. 47 (2006) 672–677.
[9] T. Schepis, M. Marwan, T. Pflederer, M. Seltmann, D. Ropers, W.G. Daniel, et al., Quantification of non-calcified coronary atherosclerotic plaques with dual-source computed tomography: comparison with intravascular ultrasound, Heart 96 (2010) 610–615.
[10] M.A. De Graaf, A. Broersen, P.H. Kitslaar, C.J. Roos, J. Dijkstra, B.P. Lelieveldt, et al., Automatic quantification and characterization of coronary atherosclerosis with computed tomography coronary angiography: cross-correlation with intravascular ultrasound virtual histology, Int. J. Cardiovasc. Imaging 29 (2013) 1177–1190.
[11] M.M. Jawaid, A. Riaz, R. Rajani, C.C. Reyes-Aldasoro, G. Slabaugh, Framework for detection and localization of coronary non-calcified plaques in cardiac CTA using mean radial profiles, Comput. Biol. Med. 89 (2017) 84–95.
[12] M.G. Dalager, M. Bøttcher, G. Andersen, J. Thygesen, E.M. Pedersen, L. Dejbjerg, et al., Impact of luminal density on plaque classification by CT coronary angiography, Int. J. Cardiovasc. Imaging 27 (April 01 2011) 593–600.
[13] A.J. Brown, D.R. Obaid, C. Costopoulos, R.A. Parker, P.A. Calvert, Z. Teng, et al., Direct comparison of virtual-histology intravascular ultrasound and optical coherence tomography imaging for identification of thin-cap fibroatheroma, Circulation: Cardiovasc. Imaging 8 (2015) e003487.
[14] H.M. Garcìa-Garcìa, B.D. Gogas, P.W. Serruys, N. Bruining, IVUS-based imaging modalities for tissue characterization: similarities and differences, Int. J. Cardiovasc. Imaging 27 (2011) 215–224.
[15] A. Nair, M.P. Margolis, B.D. Kuban, D.G. Vince, Automated coronary plaque characterisation with intravascular ultrasound backscatter: ex vivo validation, EuroIntervention: J. EuroPCR Collab. Work. Group Interventional Cardiol. Eur. Soc. Cardiol. 3 (2007) 113–120.
[16] C.M. Campos, R.J. Fedewa, H.M. Garcia-Garcia, D.G. Vince, M.P. Margolis, P.A. Lemos, et al., Ex vivo validation of 45 MHz intravascular ultrasound backscatter tissue characterization, Eur. Heart J. Cardiovasc. Imaging 16 (2015) 1112–1119.
[17] R. Manniesing, M.A. Viergever, W.J. Niessen, Vessel enhancing diffusion: a scale space representation of vessel structures, Med. Image Anal. 10 (2006) 815–825.
[18] A.F. Frangi, W.J. Niessen, K.L. Vincken, M.A. Viergever, Multiscale vessel enhancement filtering, International Conference on Medical Image Computing and Computer-Assisted Intervention, 1998, pp. 130–137.
[19] G. Ayers, J.C. Dainty, Iterative blind deconvolution method and its applications, Opt. Lett. 13 (1988) 547–549.
[20] M. Ohkubo, S. Wada, S. Ida, M. Kunii, A. Kayugawa, T. Matsumoto, et al., Determination of point spread function in computed tomography accompanied with verification, Med. Phys. 36 (2009) 2089–2097.
[21] G. Schwarzband, N. Kiryati, The point spread function of spiral CT, Phys. Med. Biol. 50 (2005) 5307.
[22] A.M. Castillo-Amor, C.A. Navarro-Navia, A.J. Cadena-Bonfanti, S.H. Contreras-Ortiz, Reduction of blooming artifacts in cardiac CT images by blind deconvolution and anisotropic diffusion filtering, 11th International Symposium on Medical Information Processing and Analysis, 2015, p. 96810P.
[23] C. Metz, M. Schaap, A. Weustink, N. Mollet, T. Van Walsum, W. Niessen, Coronary centerline extraction from CT coronary angiography images using a minimum cost path approach, Med. Phys. 36 (2009) 5568–5579.
[24] T.F. Chan, L.A. Vese, Active contours without edges, IEEE Trans. Image Process. 10 (2001) 266–277.
[25] T. Chan, W. Zhu, Level set based shape prior segmentation, 2005 IEEE Computer Society Conference on Computer Vision and Pattern Recognition (CVPR'05), 2005, pp. 1164–1170.
[26] R.T. Whitaker, A level-set approach to 3D reconstruction from range data, Int. J. Comput. Vis. 29 (1998) 203–231.
[27] W.E. Lorensen, H.E. Cline, Marching cubes: a high resolution 3D surface construction algorithm, ACM Siggraph Computer Graphics, 1987, pp. 163–169.
[28] C.V. Bourantas, I.C. Kourtis, M.E. Plissiti, D.I. Fotiadis, C.S. Katsouras, M.I. Papafaklis, et al., A method for 3D reconstruction of coronary arteries using biplane angiography and intravascular ultrasound images, Comput. Med. Imag. Graph. 29 (2005) 597–606.
[29] E.K. Oikonomou, M. Marwan, M.Y. Desai, J. Mancio, A. Alashi, E.H. Centeno, et al., Non-invasive detection of coronary inflammation using computed tomography and prediction of residual cardiovascular risk (the CRISP CT study): a post-hoc analysis of prospective outcome data, The Lancet 392 (2018) 929–939.
[30] R. Virmani, A.P. Burke, A. Farb, F.D. Kolodgie, Pathology of the vulnerable plaque, J. Am. Coll. Cardiol. 47 (2006) C13–C18.
[31] U.N. Ibebuogu, K. Nasir, A. Gopal, N. Ahmadi, S.S. Mao, E. Young, et al., Comparison of atherosclerotic plaque burden and composition between diabetic and non diabetic patients by non invasive CT angiography, Int. J. Cardiovasc. Imaging 25 (2009) 717–723.
[32] U.C. Broedl, C. Lebherz, M. Lehrke, R. Stark, M. Greif, A. Becker, et al., Low adiponectin levels are an independent predictor of mixed and non-calcified coronary atherosclerotic plaques, PLoS One 4 (2009) e4733.
[33] V.I. Kigka, G. Rigas, A. Sakellarios, P. Siogkas, I.O. Andrikos, T.P. Exarchos, et al., 3D reconstruction of coronary arteries and atherosclerotic plaques based on computed tomography angiography images, Biomed. Signal Process. Control 40 (2018) 286–294.
[34] A.W. Leber, A. Knez, A. Becker, C. Becker, F. von Ziegler, K. Nikolaou, et al., Accuracy of multidetector spiral computed tomography in identifying and differentiating the composition of coronary atherosclerotic plaques: a comparative study with intracoronary ultrasound, J. Am. Coll. Cardiol. 43 (2004) 1241–1247.
[35] M. Petranovic, A. Soni, H. Bezzera, R. Loureiro, A. Sarwar, C. Raffel, et al., Assessment of nonstenotic coronary lesions by 64-slice multidetector computed tomography in comparison to intravascular ultrasound: evaluation of nonculprit coronary lesions, J. Cardiovasc. Comput. Tomogr. 3 (2009) 24–31.
[36] Y. Wang, P. Liatsis, A fully automated framework for segmentation and stenosis quantification of coronary arteries in 3D CTA imaging, 2009 Second International Conference on Developments in eSystems Engineering, 2009, pp. 136–140.
[37] B. Bouraoui, C. Ronse, J. Baruthio, N. Passat, P. Germain, 3D segmentation of coronary arteries based on advanced mathematical morphology techniques, Comput. Med. Imag. Graph. 34 (2010) 377–387.
[38] R. Shahzad, H. Kirişli, C. Metz, H. Tang, M. Schaap, L. van Vliet, et al., Automatic segmentation, detection and quantification of coronary artery stenoses on CTA, Int. J. Cardiovasc. Imaging 29 (2013) 1847–1859.
[39] S.-T. Chen, P.-K. Hung, M.-S. Lin, C.-Y. Huang, C.-M. Chen, T.-D. Wang, et al., DWT-based segmentation method for coronary arteries, J. Med. Syst. 38 (2014) 55.
[40] S.-T. Chen, T.-D. Wang, W.-J. Lee, T.-W. Huang, P.-K. Hung, C.-Y. Wei, et al., Coronary arteries segmentation based on the 3D discrete wavelet transform and 3D neutrosophic transform, BioMed Res. Int. 2015 (2015) 798303-798303.
[41] Y. Cheng, X. Hu, J. Wang, Y. Wang, S. Tamura, Accurate vessel segmentation with constrained B-snake, IEEE Trans. Image Process. 24 (2015) 2440–2455.
[42] Y. Kitamura, Y. Li, W. Ito, H. Ishikawa, Coronary lumen and plaque segmentation from CTA using higher-order shape prior, International Conference on Medical Image Computing and Computer-Assisted Intervention, 2014, pp. 339–347.
[43] L. Athanasiou, G. Rigas, A.I. Sakellarios, T.P. Exarchos, P.K. Siogkas, C.V. Bourantas, et al., Three-dimensional reconstruction of coronary arteries and plaque morphology using CT angiography–comparison and registration with IVUS, BMC Med. Imaging 16 (9) (2016).
[44] S.S. Halliburton, P. Schoenhagen, A. Nair, A. Stillman, M. Lieber, E.M. Tuzcu, et al., Contrast enhancement of coronary atherosclerotic plaque: a high-resolution, multidetector-row computed tomography study of pressure-perfused, human ex-vivo coronary arteries, Coron. Artery Dis. 17 (2006) 553–560.
[45] R. Medina, A. Wahle, M.E. Olszewski, M. Sonka, Three methods for accurate quantification of plaque volume in coronary arteries, Int. J. Cardiovasc. Imaging 19 (2003) 301–311.
[46] A. Sakellarios, C.V. Bourantas, S.-L. Papadopoulou, Z. Tsirka, T. de Vries, P.H. Kitslaar, et al., Prediction of atherosclerotic disease progression using LDL transport modelling: a serial computed tomographic coronary angiographic study, Eur. Heart J. Cardiovasc. Imaging 18 (2016) 11–18.
[47] C.V. Bourantas, S.-L. Papadopoulou, P.W. Serruys, A. Sakellarios, P.H. Kitslaar, P. Bizopoulos, et al., Noninvasive prediction of atherosclerotic progression: the PROSPECT-MSCT study, JACC (J. Am. Coll. Cardiol.): Cardiovasc. Imaging 9 (2016) 1009–1011.